Sixth International Symposium on Turbulence and Shear Flow Phenomena
Seoul, Korea, 22-24 June 2009

THE SUSPENSION OF A SPHERE IN A TURBULENT JET

Samuel Davoust and Laurent Jacquin
Fundamental and Experimental Aerodynamics Department,
ONERA
8 rue des Vertugadins, 92190 Meudon, France
samuel.davoust@onera.fr, laurent.jacquin@onera.fr

ABSTRACT

We present an experimental study of a sphere freely suspended in a vertical turbulent jet. The sphere undergoes horizontal and vertical oscillations. The evolution of the mean equilibrium position, amplitudes and frequencies of the oscillating motion are described and the governing parameters are identified. Experimental results are used to investigate the origin of the lift force that attracts the sphere toward the jet axis. Finally, the role of the jet's turbulence on the system is considered. A model is proposed which links the amplitude of the sphere oscillations to external turbulent forcing.

INTRODUCTION

Suspending a sphere with a jet of air is a spectacular experiment that can be conducted with a light sphere and a hair dryer. While the drag of the sphere acts against gravity, a lift force brings it toward the axis of the jet. When it is tilted the sphere remains caught in the jet until a critical angle is attained. Behind what seems a perfect class room example for fluid mechanics hides a complex set of phenomena, from the creation of lift around a sphere to the interaction of a sphere with an unsteady, fully turbulent flow.

Interestingly, that phenomena has been studied by O. Reynolds in 1870. Nearly a century later, Goldshtik and Sorokin (1966) initiated a series of theoretical studies of this flow and in 1996, Feng and Joseph conducted experiments focused on the rotation of the sphere in inclined jets.

In the present study, we consider the case of a sphere suspended in a vertical turbulent jet–see Figure 2. In that case, the suspended sphere continuously oscillates vertically and horizontally. Figure 3 shows a typical time record of the horizontal and vertical position of the sphere. Notations are defined in Figure 1. This experiment can be related to two ongoing research efforts. Firstly, recent studies have aimed at understanding the effect of turbulence on a single particle or bubble. Bagchi and Balachandar (2003) studied the lift and drag fluctuations of a particle in an isotropic turbulence with numerical simulation. They showed that standard drag prevision failed for a particle larger than the smallest turbulent scales. Similar channel flows were computed by Zeng et al., (2007) considering particles

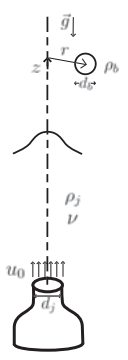

Figure 1: Definitions

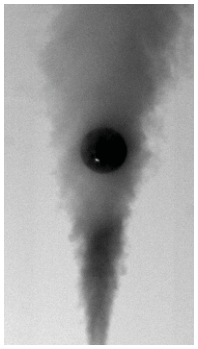

Figure 2: Sphere suspended in the jet visualized with smoke

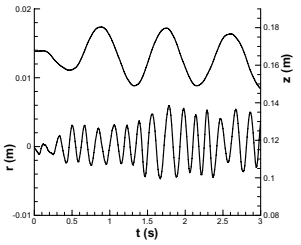

Figure 3: Time record of the vertical (top) and horizontal (bottom) sphere position.

mean Reynolds numbers Re_b below 500 and particle diameter to Kolmogorov dissipation scale ratio d_b/η below 10. Our experiment concerns other regions, the sphere Reynolds number being comprised between 10^4 and 10^5 and d_b/η is above 5000. Fluid-structure interaction is the second relevant topic. In particular, our experiment resembles a spring-mounted cylinder set in another cylinder's wake as considered by Bokaian and Geoola (1984). The wake flow experienced by the downstream cylinder is similar to the jet flow for the sphere. The effect of turbulence on such systems has not yet been fully described.

In a first section, we briefly present the experimental set-up and we describe the behavior of the system. Next, we show how do the parameters of the system govern the characteristics of the sphere's motion, specifically its mean position in the jet and the frequencies and amplitude of its oscillations. We then introduce a model that describes the effects of the jet's turbulence on the motion.

DESCRIPTION OF THE EXPERIMENT

Control parameters

As schematically described by Figure 1, the system has 7 dimensional parameters: the jet's exit velocity u_0, the sphere's and jet's diameter d_b and d_j, their respective density ρ_s and ρ_j, the gravitational acceleration g and the air's viscosity ν. We can vary these parameters, by changing the jet's exit velocity u_0, the exit nozzle diameter d_j, the sphere's d_b and ρ_b, see Table 1. Our spheres are plastic marbles of density $\rho_b = 830\ kg.m^{-3}$ except the largest one, a tennis table ball the density of which is $110\ kg.m^{-3}$.

Table 1: Sphere and jet diameters, associated symbols

$d_j \downarrow \diagdown d_b \rightarrow$	14.0 *mm*	16.0 *mm*	18.0 *mm*	20.0 *mm*	35.8 *mm*
5.53 *mm*	×	△	○	▽	□
8.74 *mm*		▲		▼	■
12.36 *mm*			●	▼	■
20.00 *mm*					♦

Non dimensional problem

From the seven dimensional parameters of our system, four independent non-dimensional parameters can be built. The two first ones are the density and diameter ratios, $K = \frac{\rho_b}{\rho_j}$ and $D = \frac{d_b}{d_j}$. K is either 85 or 700. As a result, buoyancy force and added mass effects can be neglected. D is ranging from 1.5 to 7. There seem to be a minimal value $D \approx 0.6$ below which the sphere cannot stay in the jet.

A third parameter is the jet Reynolds number, $Re_j = \frac{u_0 d_j}{\nu}$. In our experiments, Re_j varies from 5×10^4 to 11×10^4. In that range, the free jet flow keeps the same turbulent and self-similar characteristics so we do not expect this parameter to play an important role. The local sphere Reynolds number $Re_b = \frac{u(z) d_b}{\nu}$ varies from 3×10^4 to 5.5×10^4 and its influence can also be neglected.

A fourth parameter is the Froude number which compares the sphere weight to the incoming flow momentum, $F = \frac{u_0}{\sqrt{g d_j}}$. F ranges from 100 to 500.

The jet flow problem is described by $\frac{z}{d_j}$. We assume the mean jet flow to be self-similar above $\frac{z}{d_j} = 15$, a value lower than recommended by Wygnanski and Fiedler (1969) but which remains acceptable. We choose the virtual origin z_0 of each jet to be the common origin for all distances. As a result, the self-similar jet mean flow verifies $\frac{\delta(z)}{d_j} = a\frac{z}{d_j}$ and $\frac{u(r,z)}{u_0} = b\frac{d_j}{z} h(\frac{\delta(z)}{z})$. $\delta(z)$ is the jet half width. The growth rate a is close to 0.1, while b which governs the decreasing axial velocity and close to 6 (Panchapakesan and Lumley, 1993). h is a function of the jet similarity variable $\frac{\delta(z)}{z}$.

The local geometry of the sphere and jet flow is best described by the ratio of the jet width $\delta(z)$ to the sphere diameter d_b. The reference length scale of the problem is therefore chosen as $l = d_b$. For example, in non-dimensional form, the mean sphere height is:

$$Z_m = \frac{z_m}{d_b} \tag{1}$$

The reference time scale is taken as the period of a pendulum of length d_b, $t = \sqrt{\frac{d_b}{g}}$. The non-dimensional oscillation frequencies are defined as f_r and f_z. The last dimension is indeed the sphere mass m.

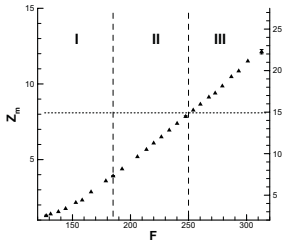

Figure 4: Evolution of mean height Z_m (left) and $\frac{z_m}{d_j}$ (right) as a function of F.

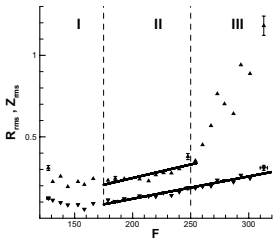

Figure 5: Evolution of the position rms. R_{rms} (▼) and Z_{rms} (▲).

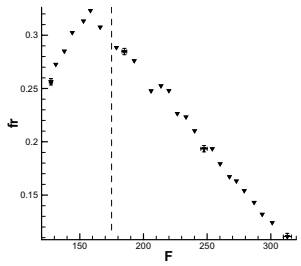

Figure 6: Evolution of the horizontal frequency f_r.

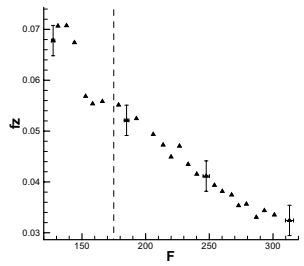

Figure 7: Evolution of the horizontal frequency f_z.

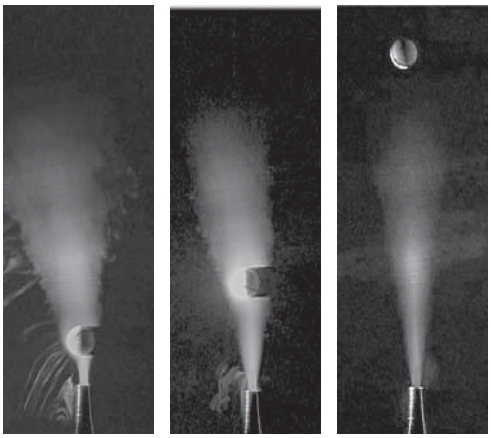

Figure 8: Flow visualisations: (a) regime I, (b) regime II, (c) regime III. Light is emitted from the left.

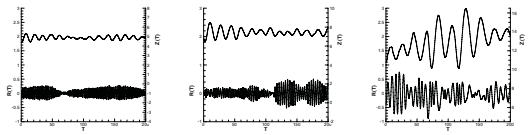

Figure 9: Time record of the vertical (top) and horizontal (bottom) sphere position in regime I (a), II (b) and II (c).

Measurements

The parameters of the jet flow are controled from the pressure and temperature measures in the jets' settling chambers.

The horizontal and vertical position $r(t)$ and $z(t)$ of the spheres are deduced from high speed films. Although the motion is three dimensional, the axial symmetry of the system enables us to capture main features of the sphere oscillatory motion through two dimensional views such as those in Figure 2. The calibration process provides us with the position of the sphere's center relatively to the center of the jet's exit nozzle with a relative precision within 1%.

The sampling frequency of is 100 frames per seconds, each acquisition lasting 130 s. This enables to capture all the times scales of the motion with precision smaller than 1.5% on the mean position and 5% on the standard deviation. Spectral analysis of the signal is used to determine the oscillation frequencies.

Description of the motion

For a given sphere and jet flow, varying the exit velocity u_0 produces different types of behavior. In this part, the flow is described by considering one single set of jet and sphere: $d_b = 16\ mm$ and $d_j = 8.74\ mm$. The results are presented in non dimensional form. Figures 4 to 7 show the evolution of mean vertical position Z_m, the horizontal and vertical position rms R_{rms} and R_{rms}, and the oscillation frequencies f_r and f_z.

Figures 4 and 5 suggest a segmentation of the data into three different regimes. Figures 8(a) to 8(c) provide flow visualizations of the flow in each case while Figures 9(a) to 9(c) show sample trajectories. Finally, Figure 10 shows a synthetic plot comparing the jet half-width to the positions of the sphere in the three different regimes. Theses regimes will now be described.

Regime I: Large sphere behavior. From $F = 120$ to 175, the sphere is located in the development region of the turbulent jet. Figure 10 shows that the sphere is larger than the local jet width.

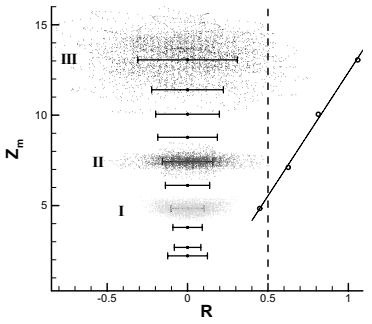

Figure 10: Scatter plots of the sphere position for the three different regimes. The horizontal bars gives the rms amplitude at different mean height. The full line on the right is the jet half-width. Vertical dashed line is the sphere radius.

The jet flow is thickened by the sphere and considerably deflected as the sphere moves aways from the jet's axis (Figure 8(a)). The mean height Z_m grows non-linearly (Figure 4), while the position rms remains almost constant (Figure 5). As seen in Figure 6 and Figure 7, the frequencies of the horizontal and vertical oscillations evolve in a puzzling non monotonous way.

Regime II: Regular behavior. From $F = 175$ to 250, the mean position of the sphere begins to enters the self-similar region of the free jet. In this region, the mean velocity on the axis, $u(Z_m)$ behaves as u_0/Z_m. Considering that the drag force felt by the sphere at height Z_m is roughly proportional to $u^2(Z_m)$, and equilibrates the weight of the sphere, Z_m should be proportional to u_0. This is confirmed by the linear behavior obtained in Figure 4.

Figure 6 and 7 show that the oscillation frequencies decrease regularly from 0.3to 0.1 for f_r and from 0.055 to 0.035 for f_z. Note that these frequencies are much lower than the frequencies associated with the jet and sphere flow's turbulence. As Figure 5 shows, in that range R_{rms} and Z_{rms} grow linearly with the same rate, until $F = 250$. Then Z_{rms} suddenly explodes. Flow visualizations such that of Figure 8(b) reveal that the jet is still significantly deflected by the sphere. Figure 10 proves that the sphere's radius is now smaller than the local jet's half width.

Regime III: Chaotic behavior. Above $F = 250$, the motion looses regularity, as shown by the trajectory plotted in Figure 9(c). The sphere is now small compared to the local jet width, see Figures 8(c) and 10. Large amplitude events occur, the sphere being rather unstable in the jet. An example of a trajectory is shown in Figure 11: the sphere falls down half it's mean height before being caught back in the jet. This type of event leads to large vertical rms Z_{rms} as shown in Figure 5. Surprisingly, the mean height, the horizontal rms and the main oscillation frequencies keep evolving in the same regular way as before. At last, Figure 10 shows that the jet grows faster than the horizontal position rms. The amplitude of the oscillations remains smaller than the jet width.

In the next section, we will compare different configurations to understand the general mechanisms of the system.

NON DIMENSIONAL STUDY

In this section we present all the experimental data using non dimensional variables in order to identify general characteristics of the motion. In order to compare the motion of sphere for a generic jet-flow, we limit ourselves to motions of spheres located in regions where the jet may be considered self-similar ($z_m \geq 15 d_j$). For the

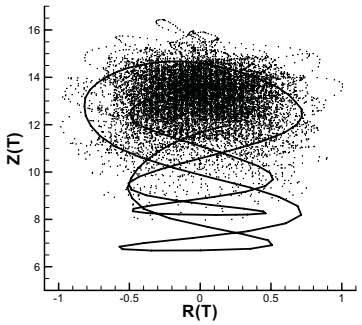

Figure 11: Scatter-plot and a trajectory exhibiting an extremely large variation of sphere position.

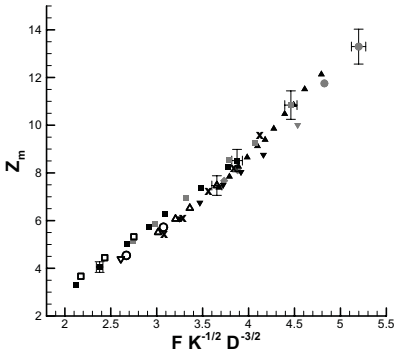

Figure 12: Evolution of Z_m as a function of $\frac{F}{\sqrt{KD^3}}$.

particular case detailed above, the data that remains is limited to the regime III, above the dotted line shown in Figure 4. The large variation of the parameters (Table 1) insures that Regime I and II remain included in the following analysis. Although the flow was not yet self-similar, the previous description of Regime I and II remains valid.

Mean height

If we consider locally a self-similar jet flow profile of maximum velocity $u(z)$, half-width $\delta(z)$ and a sphere of diameter d_b located on the axis ($r = 0$) of that flow, the drag $F_z(r, z)$ of the sphere verifies:

$$\frac{F_z(0,z)}{\frac{1}{2}\rho_j \pi \frac{d_b^2}{4} u(z)^2} = C_z\left(\frac{\delta(z)}{d_b}\right) \tag{2}$$

through its argument the drag coefficient C_z depends on Z_m, see (1). The present problem differs from the classical case of a sphere immersed in an uniform flow. At equilibrium, we have $z = z_m$ and $F_z(0, z_m) = mg = \frac{4}{3}\pi \frac{d_b^3}{8} \rho_b g$. Using the jet flow assumptions and (1) we get:

$$Z_m = \frac{F}{\sqrt{KD^3}} \sqrt{\frac{3b^2}{4} C_z(Z_m)} \tag{3}$$

Through relation (3), Z_m depends on $\frac{F}{\sqrt{KD^3}}$. The mean height of the sphere corresponds to the position where the jet flow momentum equilibrates the sphere weight.

Figure 12 shows Z_m as a function of $\frac{F}{\sqrt{KD^3}}$ for the different configurations described in Table 1. A good correlation is obtained. The drag coefficient C_z, not shown here, is found to increase linearly from 0.1 to 0.3 with Z_m, across the entire range. Even for high Z_m, C_z has not reached an asymptotic value.

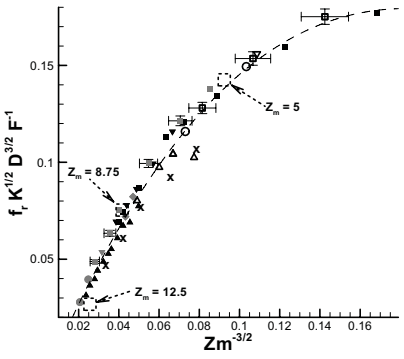

Figure 13: Non-dimensional frequency f_r.

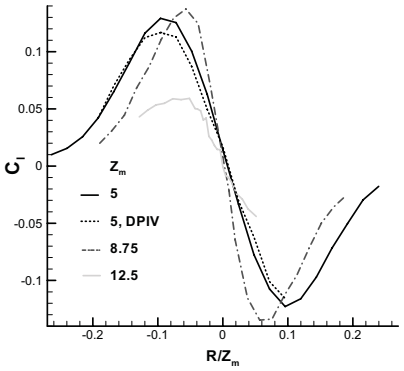

Figure 14: Lift coefficient C_l as a function of r/z_m for Z_m/D = 5, 8.75 and 12.5.

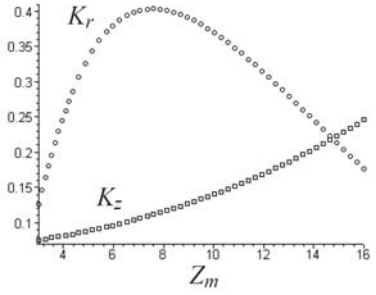

Figure 15: Lift and drag force constants K_r (○) and K_z (□)

Horizontal oscillation frequency

For a sphere located at a distance r from the center of a self-similar jet profile at height z_m, the lift force $F_r(r, z_m)$ fulfills:

$$\frac{F_r(r,z_m)}{\frac{1}{2}\rho_j \pi \frac{d_b^2}{4} u(z_m)^2} = C_l\left(\frac{\delta(z_m)}{d_b}, \frac{r}{\delta(z_m)}\right) \quad (4)$$

A Taylor expansion around $r = 0$ gives

$$\frac{F_r(r,z_m)}{\frac{1}{2}\rho_j \pi \frac{d_b^2}{4} u(z_m)^2} \approx -K_r(Z_m) \times \frac{r}{\delta(z_m)} \quad (5)$$

K_r is the non-dimensional lift force constant and is function only of the local sphere to jet width ratio Z_m defined in (1). This leads us to introduce an oscillation pulsation ω_r for a sphere of mass m related to a physical spring-constant $m\omega_r^2$ so that:

$$-F_r(r,z_m) = \frac{1}{2}\rho_j \pi \frac{d_b^2}{4} u(z_m)^2 K_r(Z_m) \times \frac{r}{\delta(z_m)} = m\omega_r^2 \times r \quad (6)$$

Replacing m by $\frac{4}{3}\pi\rho_b d_b^3$ and converting the pulsation into the non-dimensional horizontal oscillation frequency $f_r = \frac{1}{2\pi}\omega_r \sqrt{\frac{d_b}{g}}$, we get:

$$f_r \frac{\sqrt{KD^3}}{F} = \frac{1}{2\pi} Z_m{}^{-3/2} \sqrt{\frac{3b^2}{4a} K_r(Z_m)} \quad (7)$$

Experimental results shown in Figure 13 confirm that $f_r \frac{\sqrt{KD^3}}{F}$ reduces to a function of $Z_m^{-3/2}$, in accordance with (7). The dependence of K_r on Z_m is commented below. A similar approach can also be followed for the vertical frequency f_z.

Nature of the lift force. Two physical mechanism may be referred to for understanding the lift force experienced by the sphere, although the present flow is probably too complex be be fully represented by either one.

For a sphere larger than the jet (Regime I, $Z_m < 6$, Figure 10), the phenomenon that is visually observed (Fig 8(a)) is the deflection of the jet by the sphere. This refers to the Coanda effect. By reaction, the jet deflection attracts the sphere toward the center of the jet. Experimental studies conducted with plane jets over cylinders by Newman (1961) show that the position of separation is governed by the initial ratio of jet width to cylinder diameter. In our case, the mechanism is three dimensional, a situation which has little been studied before. A mean velocity profile made with Digital Particle Imagery Velocimetry (DPIV) one diameter behind the sphere shows that the deflection of the jet (the lift force) is organized at first into a vortex pair. This pair later disappears and the flow collapses into an almost uniform deflection of the jet.

Now, when the sphere becomes relatively small compared with the jet's half-width the problem evolves toward that of a sphere in a shear flow. An analytical expression for the lift of a small inviscid shear on the sphere was derived by Auton (1987) and yields a lift force proportional to the shear intensity. In that case, the sphere is displaced toward high velocities that is, in our case toward the center of the jet. This is defined by Auton (1987) as positive lift. However, numerical simulations by Kurose and Komori (1999) for $Re_b \leq 500$, and experiments by Yamamoto and al. (1993) fot $Re_b \leq 3.5 \times 10^4$ show that the lift force is now negative that is toward small velocities. As pointed out by Sakamoto and Haniu (1995), vortex shedding process in the shear could explain this negative lift. Numerical simulations by Zeng et al. (2007) of a sphere in a turbulent channel flow show the same behavior. Finally, in the system of two cylinders in tandem in a cross-flow, the downstream cylinder experiences a lift force oriented toward the center of the other cylinder's wake (Bokaian and Geoola 1984), again a negative lift force.

We evaluated the lift force on the sphere using both the DPIV data and traditional force measurements for Z_m = 5, 8.75 and 12.5. With DPIV, the mean lift force is found by integrating the transverse momentum flux behind the sphere. The lift coefficient as defined in (4) is plotted in Figure 14. There is a good agreement between the two types of force measurements for $Z_m = 5$. For all Z_m, the curves have a similar behavior indicating that in that range a positive lift, of the Coanda type, dominates. As described above, the slope K_r of the lift force around $r = 0$ transforms into a non-dimensional oscillation frequency, see (6). The frequencies calculated from the slope of the lift force are shown as the arrow indicated dashed squares on Figure 13. There is excellent agreement with the recorded oscillation frequencies. This validates a linear oscillator model across most of the experimental data.

Inversely, the frequency data shown in Figure 13 may be used to determine the non dimensional lift force constant defined in (5). The results is shown in Figure 15. K_z, the vertical counterpart to K_r is

evaluated the same way and also shown. K_r reaches a maximum for $Z_m = 8$ and then decreases. However, the evolution of K_r does not prelude a negative lift force until beyond $Z_m = 20$. The negative shear lift regime could not be reached in our experiment nor measured: for large Z_m, the deflection of the jet became too small to set a reliable lift force. On the other hand, the vertical force constant K_z increases monotonously, like C_z, and overcomes K_r.

TURBULENCE FORCED OSCILLATOR

Formulation

In this section, we investigate to what extent may the system be described by an harmonic oscillator model. Neglecting the azimuthal motion of the sphere, the linearized equations of motion can be written in non dimensional form as:

$$\ddot{R} + 2\xi_r\Omega_r\dot{R} + \Omega_r^2 R = \frac{F_{r,ext}}{mg} + \Upsilon_{rz}\Omega_r^2 Z \tag{8}$$

$$\ddot{Z} + 2\xi_z\Omega_z\dot{Z} + \Omega_z^2 Z = \frac{F_{z,ext}}{mg} + \Upsilon_{zr}\Omega_z^2 R \tag{9}$$

Using (3) and (7), the oscillation pulsations are:

$$\Omega_r^2 = \frac{1}{a}\frac{K_r}{C_z}\frac{1}{Z_m} \tag{10}$$

$$\Omega_z^2 = 2\frac{K_z}{C_z}\frac{1}{Z_m} \tag{11}$$

Concerning the damping terms ξ_r and ξ_z we may assume that the oscillation dynamics is much slower than the flow timescale around the sphere $\frac{d}{u}$. Under this quasi-steady assumption, linearizing drag with a perturbation velocity gives the dimensional damping forces $\frac{1}{2}\rho_j\pi\frac{d_b^2}{4}C_z u(z)\dot{r}$ and $\frac{1}{2}\rho_j\pi\frac{d_b^2}{4}C_z 2u(z)\dot{z}$. In non-dimensional form, we obtain the following damping ratios:

$$\xi_r = \sqrt{\frac{3a}{16}}\frac{1}{\sqrt{K}}\frac{C_z}{\sqrt{K_r}}\sqrt{Z_m} \tag{12}$$

$$\xi_z = \sqrt{\frac{3}{8}}\frac{1}{\sqrt{K}}\frac{C_z}{\sqrt{K_z}}\sqrt{Z_m} \tag{13}$$

These are small quantities that depend on K and which grow with Z_m. Our system is lightly damped. $F_{r,ext}$ and $F_{z,ext}$ are external forces due to the jet's turbulence. Finally Υ_{rz} and Υ_{zr} are constants representing interaction between the horizontal and vertical motions.

Excitation force, frequency cutoffs and resonance

In this part, we propose a description of the oscillations rms through a spectral study of the oscillator equations (8)-(9) considering the role of the turbulent forcing terms $F_{r,ext}$ and $F_{z,ext}$. We suppose that radial and axial turbulent velocity fluctuations v' and u' perturb the oscillator. Supposing $v' \propto u'$ and $u'/u << 1$ and similarly, that turbulent structures of size $l > d_b$ have a large timescale l/u' compared to the mean flow time scale d_b/u, the linearized lift and drag perturbations due to turbulence gives the following forcing term in (8) and (9):

$$\frac{F_{r,ext}}{mg} = \frac{2u'C_l/C_z + v'}{u(z_m)} \approx \frac{v'}{u(z_m)} \tag{14}$$

$$\frac{F_{z,ext}}{mg} = \frac{2u'}{u(z_m)} \tag{15}$$

The forcing terms reduce to the turbulent velocities fluctuations rates. Spectral density D_u of the axial fluctuations is shown in Figure 16 as a function of $St = f\frac{u(z)}{\delta(z)}$. This axial velocity fluctuation spectrum has been obtained using a single hot wire DANTEC 55P11 on the jet

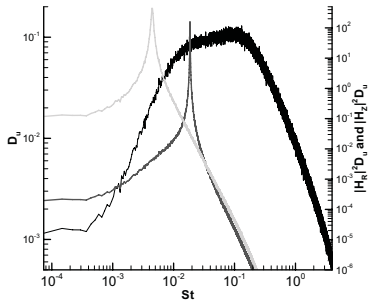

Figure 16: Spectral density D_u (−) as a function of $St = f\frac{u(z)}{\delta(z)}$. Spectral responses $|H^R|^2 D_u$ (−) and $|H^Z|^2 D_u$ (−)

axis at $z/d_j = 35$ with $u(z) = 19.6m.s^{-1}$ and $\delta(z) = 1.65 \times 10^{-2}m$. The spectra have been obtained using 200 data blocks, acquired at an acquisition rate $f_{acq} = 22kHz$ and low-pass filtered at $f_c = 10kHz$. The spectra peaks around $St = 0.2$, which corresponds to the jet large scale structures (Tso and Hussain, 1989). Above that, the turbulent energy decreases as $St^{-5/3}$. Taking the Fourrier transform of (8) without the coupling term, we obtain the classical result for R_{rms}:

$$R_{rms}^2 = \int_0^{+\infty} |H^R(\omega)|^2 D_v(\omega)d\omega \tag{16}$$

with $|H^R(\omega)|^2 = \frac{1}{(\Omega_r^2-\omega^2)^2+(2\xi_r\Omega_r\omega)^2}$ the transfer function of the horizontal oscillator. Here D_v is the spectral density of the radial velocity fluctuation. The spectral response of the horizontal and vertical oscillator for $K = 700$ and $Z_m = 8$ is also shown in Figure 16, with D_v approximated as $\frac{v'^2}{u'^2}D_u$ using the self-similar turbulent intensities u' and v' measured by Panchapakesan and Lumley (1993). The peaks, representing the oscillations frequencies, occur in a very low jet frequency zone which is associated to large scale intermittent events.

The sphere should not be receptive to turbulent structures smaller than its size, because it averages them out. Therefore, it acts as a low-pass filter with a cutoff frequency ω_c. With the cutoff, the spectral density of the excitation D_v is changed into:

$$D_v^c(\omega) = \frac{D_v(\omega)}{1 + (\omega/\omega_c)^\alpha} \tag{17}$$

where α represents the steepness of the low pass filter. The cutoff frequency St_c above which the turbulent eddies are filtered out verifies $St_c \propto \frac{u'}{u(z)}\frac{\delta(z)}{d_b} = a\frac{u'}{u}Z_m$ with $\frac{u'}{u}$ the axial turbulence level in a jet, around 0.25 (Panchapakesan and Lumley, 1993). Transforming ω into St with $\omega = \frac{b}{a}\frac{F}{D^{3/2}}\frac{1}{Z_m^2} \times St$, we use (3), (10) to (13) to find:

$$R_{rms} = aZ_m\left(\int_0^{+\infty}\frac{D_v^c(St)}{(\frac{K_r}{C_z} - St^2\frac{4}{3a}K\frac{1}{C_z}\frac{1}{Z_m})^2 + (St)^2}dSt\right)^{1/2} \tag{18}$$

$$Z_{rms} = aZ_m\left(\int_0^{+\infty}\frac{2D_u^c(St)}{(2a\frac{K_z}{C_z} - St^2\frac{4}{3a}K\frac{1}{C_z}\frac{1}{Z_m})^2 + (2St)^2}dSt\right)^{1/2} \tag{19}$$

The same approach has been used for Z_{rms}. In Figure 17, R_{rms} and Z_{rms} given by (18) and (19) are compared to experimental results. This model gives a correct prediction of the position rms up to $Z_m = 8$. K is chosen as 700, and the choice of the low pass filter does not influence significantly the results because the oscillator is itself a low pass filter. D_v was again approximated by $\frac{v'^2}{u'^2}D_u$.

As the sphere rises, the jet's most energetic frequencies decrease like $\frac{1}{Z_m}$, faster than the oscillation frequencies that decrease like $\frac{1}{Z_m^{1/2}}$. As a result, the oscillator captures a rising amount of energy from the jet's energy containing frequencies. As seen in Figure 17, we should expect from the model given by (18) and (19) an increase in

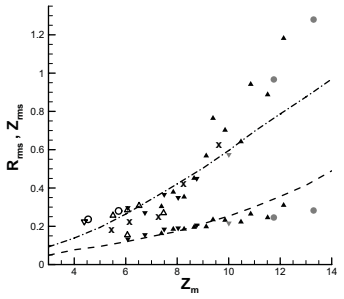

Figure 17: R_{rms} and Z_{rms} as a function of Z_m, for K = 700. Predictions given by (18) and (19) is shown in dotted line

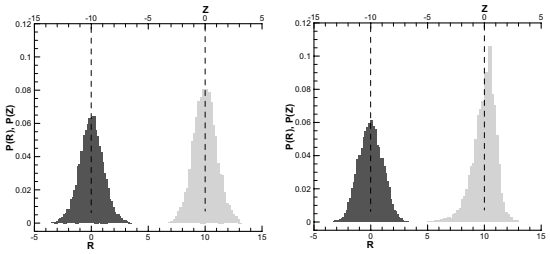

Figure 18: RMS normalized probability density functions for horizontal (■, lower axis) and vertical (■, upper axis) position. Z_m = 6: Fig. 18(a) and Z_m = 11.5: Fig. 18(b)

the slope of the horizontal rms R_{rms} first: the horizontal oscillation frequency being higher, the associated transfer function will interact with the fluctuation's spectral maximum before the vertical one (see Figure 16).

This model therefore fails to predict the dramatic increase in Z_{rms}. Nevertheless, from experimental observations like the large trajectory shown in Figure 11, we believe that the expected increase of R_{rms} is instead converted into vertical rms Z_{rms} by such intermittent events. This mechanism cannot be accounted for by our model. Figures 18(a) and 18(b) which show the histograms pf the sphere position confirm that when Z_m ins increased from 6 to 11.5, the r-pdf remains unaffected and symmetric whereas the z-pdf is skewed, with a net increase of the probability of negative z. This is due to trajectories such as that of Figure 11. These non-symmetric deviations cannot be accounted for by this model and remain unexplained.

CONCLUSION

An experiment on the suspension of a sphere in a vertical turbulent jet has been realized considering a rather large variation of the different control parameters. The behavior of the system was classified into three different regimes that depend on the relative sphere to jet-width ratio. A compilation of the experimental results has showed that the dominant parameters influencing the dynamics of the sphere in the jet have been identified and enabled a successful correlation of the data (mean equilibrium position, amplitude and frequencies of the sphere oscillatory motion). Experimental evidence suggests that the lift force remains attractive and is of the Coanda effect nature, namely a deviation of the jet flow after interaction with the sphere surface. A turbulence-forced oscillator model has been developed which represents fairly the horizontal and vertical oscillations up to a medium sphere to jet ratio. The failure of that model to explain the change of behavior that occurs beyond is linked to the apparition of intermittent events. Further studies of this type of oscillator are needed to describe this particular chaotic regime and ultimately explain the ejection of the sphere.

Auton, T. R., 1987, "The lift force on a spherical body in a rotational flow", *Journal of Fluid Mechanics*, Vol. 183, pp.199–218.

Bagchi, P. and Balachandar, S., 2003, "Effect of turbulence on the drag and lift of a particle", *Physics of Fluids*, Vol. 15, pp.3496–3513.

Blevins, R. D., 1974, "Fluidelastic whirling of a tube row", *ASME Journal of Pressure Vessel Technology*, Vol. 96, pp.263-267.

Bokaian, A. and Geoola, F., 1984, "Wake-induced galloping of two interfering circular cylinders", *Journal of Fluid Mechanics*, Vol. 146, pp.383–415.

Feng, J. and Joseph, D. D., 1996, "The motion of a solid sphere suspended by a Newtonian or viscoelastic jet", *Journal of Fluid Mechanics*, Vol. 315, pp.367–385.

Goldshtik, M. A. and Sorokin, V. N., 1966, "Rotation of a cylinder at the boundary of a jet", *Zhurnal Prikladnoi Mekhaniki i Tekhnicheskoi Fiziki*, No. 1, pp.123–124.

Kurose, R. and Komori, S., 1999, "Drag and lift forces on a rotating sphere in a linear shear flow", *Journal of Fluid Mechanics*, Vol. 384, pp.183–206.

Newman, B. G., 1961, "The deflexion of plane jets by adjacent boundaries-Coanda effect", *Boundary Layer and Flow Control: Its Principles and Application*, p.232.

Paidoussis, M. P. and Price, S.J., 1988, "The mechanisms underlying flow-induced instabilities of cylinder arrays in crossflow", *Journal of Fluid Mechanics*, Vol. 187, pp.45–59.

Panchapakesan, N. R. and Lumley, J. L., 1993, "Turbulence measurements in axisymmetric jets of air and helium. Part 1. Air jet", *Journal of Fluid Mechanics*, Vol. 246, pp.197–223.

Reynolds, O., 1870, "On the Suspension of a Ball by a Jet of Water", *Proceedings of the Manchester Literary Philosophical Society*.

Sakamoto, H. and Haniu, H., 1995, "The formation mechanism and shedding frequency of vortices from a sphere in uniform shear flow", *Journal of Fluid Mechanics*, Vol. 287, pp.151–171.

Tso, J. and Hussain, F., 1989, "Organized motions in a fully developed turbulent axisymmetric jet", *Journal of Fluid Mechanics*, Vol. 203, pp.425–448.

Wygnanski, I. and Fiedler, H., 1969, "Some measurements in the self-preserving jet", *Journal of Fluid Mechanics*, Vol. 38, pp.577–612.

Yamamoto, F. and Koukawa, M. and Monya, H. and Teranishi, A. and Miyamoto, H., 1993, "An experimental study for simulation of pneumatic conveying (lift and drag applied to a sphere in high-Reynolds-number linear shear flows)", *BJSME International Journal. Series B*, Vol. 69, pp.294–299.

Zeng, L., Balachandar, S., Fischer, P. and Najjar, F., 2007, "Interactions of a stationary finite-sized particle with wall turbulence", *Journal of Fluid Mechanics*, Vol. 594, pp.271–305.